Use of absorption optical indices to assess seasonal variability of dissolved organic matter in amazon floodplain lakes

Maria Paula da Silva[1]*, Lino A. Sander de Carvalho[2], Evlyn Novo[1], Daniel S. F. Jorge[1], Claudio C. F. Barbosa[2]

[1] Remote Sensing Division, National Institute for Space Research, 12227-010, São José dos Campos, Brazil
[2] Image Processing Division, National Institute for Space Research, 12227-010, São José dos Campos, Brazil;
Correspondence to: Maria Paula da Silva (maria-paula.da-silva@ufz.de)

Abstract. Given the importance of dissolved organic matter (DOM) in the carbon cycling of aquatic ecosystems, information on its seasonal variability is crucial. In this study we assess the use of available absorption optical indices based on in situ data to both characterize the seasonal variability of DOM in a highly complex environment and for application in large-scale studies using remote sensing data. The study area comprises four lakes located at the Mamirauá Sustainable Development Reserve (MSDR). Samples for the determination of coloured dissolved organic matter (CDOM) and remote sensing reflectance (Rrs) were acquired in situ. The Rrs was used to simulate the response of the visible bands of the Multi-Spectral Instrument (MSI)/Sentinel and used in the proposed models. Differences between lakes were tested regarding CDOM indices. The results highlight the role of the flood pulse in DOM dynamic in the flood plain lakes. The validation results showed that the proposed model using a_{CDOM} as proxy of $S_{275-295}$ during rising water is worthwhile, demonstrating its potential application to Sentinel/MSI imagery data for studying DOM dynamics on large scale studies.

1 Introduction

Floodplain is a type of wetland characterized by a mosaic of landscapes which oscillates periodically between aquatic and terrestrial systems. This oscillation represents a key aspect in the biogeochemistry, ecology and hydrology of floodplain lakes (Junk et al., 1989; Moreira-Turq et al., 2004). Among other effects, the flood pulse (*sensu* Junk et al., 1989) affects the proportion of autochthonous and allochthonous sources contributing to the dissolved organic matter (DOM) pool in floodplain lakes throughout the year (Melo et al., 2019).

DOM represents the largest pool of organic carbon in the aquatic environment and it has an important role in the ecosystem carbon budgets (Seekell et al., 2018; Tranvik et al., 2009; Richey et al., 2002). Besides that, DOM also controls light availability in the water column, playing a vital role in primary productivity of aquatic ecosystems and consequently fisheries and other food webs (Hastie et al., 2019; Maia and Volpato, 2013; Volpato et al., 2004).

DOM concentration in the environment is usually determined by the concentration of dissolved organic carbon (DOC) (Coble, 2007). However, simple measurement of DOC concentration can limit the study of the seasonal variation in the DOM quality (e.g. composition) and origin since it is related only to the bulk of DOM (Jaffé et al., 2008). Qualitative parameters are needed to better understand DOM dynamics such as ultraviolet (UV) and visible absorption measurements and fluorescence, which are an alternative for high costly laboratory analysis (Li and Hur, 2017). Helms et al., (2008) have shown that the spectral slope calculated in the range of 275 and 295 nm ($S_{275-295}$) is an indicator of DOM molecular weight and a tracer of degradation processes. The absorption coefficient of coloured dissolved organic matter (CDOM) at 350 nm (a_{CDOM} (350)), a_{CDOM} spectral slope ($S_{275-295}$) and DOC concentration have been used to study the rates of water exchange between river and floodplain on Mississippi and Atchafalaya River (Spencer et al. 2008; Shen et al., 2012).

In order to study DOM dynamics in wide spatial-temporal scale satellite images have been assessed as a source of optical information about CDOM. Many studies have used Landsat images for investigating a_{CDOM} at the different wavelengths, more commonly at 350 nm, 440 nm and 420 nm (Fichot et al., 2013; Kutser et al., 2005; Zhu et al., 2014; Brezonik et al., 2015). However, only a few studies have looked at the spectral slope of DOM. In a Pan-Arctic study, Fichot et al. (2013) showed that $S_{275-295}$ can be directly estimated from satellite images using a multi-linear parameterization of MODIS marine reflectance. However, the reflectance of water in the visible bands may not reflect changes in the spectral slope of CDOM in the UV domain as show by Vantrepotte et al. (2015) by applying Fichot et al. (2013) model in three coastal water regions. Therefore, Vantrepotte et al., (2015) proposed the use of a_{CDOM} as a proxy for $S_{275-295}$ as it proved to be less affected by water optical quality and atmospheric correction. Nonetheless, both studies (Fichot et al., 2013; Vantrepotte et al., 2015) used MODIS data whose spatial resolution (250-1000 m) restricts the application to inland water studies. In recent years the availability of Multi-Spectral Instrument (MSI) images, on board of the Sentinel-2A (June/2015) and Sentinel-2B (March/2017), has expanded the potential of remote sensing application for DOM monitoring because of its high spatial (10 and 20 m), temporal (5 days) and radiometric (12-bit) resolutions (Toming et al., 2016).

The main objectives of this study are to: i) investigate the variability of a_{CDOM} in floodplain lakes during the receding and rising phases of the Solimões River, ii) examine the potential of $S_{275-295}$ for distinguishing differences in DOM by comparing it in two hydrograph phases; and iii) propose an algorithm to estimate a_{CDOM} (440) as a proxy for $S_{275-295}$ using simulated MSI/Sentinel bands to support future application of satellite remote sensing for inland DOM studies.

2 Material and methods

2.1 Study area

The study sites are four lakes located in the floodplain built at the confluence between Solimões and Japurá rivers, near Tefé and inside the Mamirauá Sustainable Development Reserve (MSDR) (Figure 1b), a well-preserved flooded forest under low human pressure (Ayres, 1995; Castello et al., 2009; Mori et al., 2019; Queiroz, 2007). In this area, the seasonal flood is caused by both the rainfalls (in upper Amazon basin and locally-from December to May, with an average of 300 mm/month) and by the annual melt of the Andean cordillera during the austral summer (Junk, 1989). The yearly MSDR flood pulse causes, in average, 12 meters amplitude in the water level between the dry (September to November) and the flood season (May and mid-July) (Queiroz, 2007). The rising of the water level begins in January and goes up to late April while the water receding phase starts in July. During the flood period, which begins in May, the floodplain is totally occupied by water until the beginning of the receding phase (Affonso et al., 2011). The lakes were selected according to criteria defined in Jorge et al. (2017a) to guarantee access to them throughout the hydrological year and sizes compatible to the spatial resolution of the visible bands of the MSI/Sentinel2A (10 m and 20 m) . Additionally, the lakes have intrinsic differences: two of them (Buabuá and Mamirauá) are small perennial lakes surrounded by flood forest, isolated, while the others (Pantaleão and Pirarara) are lakes connected to the Japurá river along the entire hydrological year, with variable size and depth in response to the flood pulse.

2.2 Data source

Data were acquired in Buabuá, Mamirauá, Pantaleão and Pirarara lakes by the Instrumentation Laboratory for Aquatic Systems team (LabISA – http://www.dpi.inpe.br/labisa) of the National Institute for Space Research (INPE-Brazil). More details about the fieldwork and measurements are provided in Jorge et al. (2017a, 2017b).

The field campaigns were carried out in March-April and July-August of 2016 which corresponds to the rising and receding water level of Solimões River. Table 1 contains the sampling points and the DOC concentration measured. In total 87 samples were collected among the lakes and seasons.

2.3 Measurements

2.3.1 Remote sensing reflectance

The radiometric measurements to derive remote sensing reflectance (Rrs) were carried out for all sampling points, using three intercalibrated RAMSES–Trios sensors. The sensors measured above water radiance, sky radiance, and water surface irradiance, between 350 and 900 nm. During the measurements, the sensors were positioned with azimuth angles between 90° and 135° in relation to the sun and a Zenith angle of 45° to avoid sun glint effects (Mueller and Fargion, 2002). The measurement framework followed Mobley (1999). All of the measurements were made between 10:00 and 13:00 (local time) and at least 15 samples were obtained for each sample point. The dataset was processed using MSDA_XE (TRIOS, 2018) and Matlab (Mathworks, Natick, MA, USA). The Rrs estimate followed Mobley (1999), with sun glint correction based on each sampling point. The calculated Rrs was used to simulate the reflectance of the MSI bands. For this, MSI Relative Spectral Response (RSR) of the sensor was used (Equation 1):

$$R_{rs}(B_i) = \frac{\int_{\lambda_m}^{\lambda_n} RSR(\lambda) \cdot R_{rs_{m(\lambda)}} d\lambda}{\int_{\lambda_m}^{\lambda_n} RSR(\lambda) d\lambda}, \quad (1)$$

where Rrs_m is the Rrs measured in situ and Rrs (B_i) is the Rrs simulated for the i-th band of Sentinel-2A, in the wavelength range of λm to λn. MSI RSR were taken from the user guide of the sensor (https://earth.esa.int).

2.3.2 CDOM Absorption Coefficient

Water samples were filtered first through Whatman GF/F (0.7 µm) filters (burned at 400 ºC) and then through 0.22 µm pore size polycarbonate filter. The filtrated sample was stored in sterilized dark glass bottles and kept refrigerated up to 14 days until analysis. During the analysis, all samples were kept at ambient temperature. CDOM spectral absorbance was measured with a Shimadzu UV-2600 spectrophotometer in the wavelength range between 220 and 800 nm, with increments of 1 nm and converted to a_{CDOM} (λ) according to Equation (2) (Bricaud et al., 1981):

$$a_{cdom}(\lambda) = \frac{2{,}303 \cdot A(\lambda)}{L}, \qquad (2)$$

where A (λ) is the spectral absorbance of the filtered sample in the specific wavelength λ (nm) and L is the cuvette path length (0.1 m).

The average of a_{CDOM} between 750 and 800 nm was used to correct the residual absorption spectra due to baseline drift, temperature, scattering, and refractive effects (Coble, 2007).

2.3.3 Spectral slope determination

Helms et al., (2008) have shown that the spectral slope calculated in the range of 275 and 295 nm ($S_{275-295}$) is an indicator of DOM molecular weight and a tracer of degradation processes. In the present study, $S_{275-295}$ was computed according to the Equation 3 using non-linear fit (Helms et al., 2008; Bricaud et al., 1981). This function describes the a_{CDOM} (λ) behaviour along the electromagnetic spectrum and is expressed as:

$$a_{cdom}(\lambda) = a_{cdom}(\lambda_{ref}) \cdot e^{-S(\lambda-\lambda_{ref})}, \qquad (3)$$

where S is the spectral slope parameter (nm^{-1}) between the wavelength interval of $\lambda - \lambda_{ref}$ and λ_{ref} is a reference wavelength (nm).

The spectral slope ratio (S_R) between the wavelengths intervals of 275-295 nm on 350-400 nm was also computed in the same away describe in Equation 3.

2.3.4 Statistical analyses

The temporal variability of DOM was assessed using a_{CDOM} (440). This wavelength was chosen due to the high CDOM absorption at low wavelengths (Jorge et al., 2017a), being also a region used as reference in remote sensing studies, at least, in the last thirty-six years (Bricaud et al., 1981; Brezonik et al., 2015; Bukata et al.,1995; Werdell et al., 2018).

The coefficient of variance (CV) was also computed for assessing a_{CDOM} (440) variability. Kruskal Wallis test (one-way ANOVA on rank) with a significance level of 95% was applied to test the differences between lakes and hydrograph phases regarding a_{CDOM} (440) values as follows: i) in a first run, the test used the entire data set; ii) in a second run, to test the influence of Buabuá and Mamirauá samples acquired during the rising period, those samples were removed.

The mean $S_{275\text{-}295}$ of the two months representing the same hydrograph phases (e.g. July and August for receding; March and April for rising) was computed for each sampling point to analyse their variability within each lake and phase. All the statistical analysis were performed using the software Matlab (Mathworks, Natick, MA, USA).

2.3.5 Model calibration and validation

The model proposed by Vantrepotte et al. (2015) based on the ratio of a_{CDOM} (412) and parameterized according to three coastal zones was tested to our data set using a_{CDOM} (440), once the band in 412 nm is not present at MSI/Sentinel. A simple power function (Equation 4) was also tested.

$$S_{275-295} = x \cdot a_{cdom}(440)^{-y} \,, \qquad (4)$$

where x and y are fitting coefficients of the Equation (4).

Monte Carlo was applied to Equation 4 to find the coefficients and validate the model. Out of 42 $S_{275\text{-}295}$ samples collected during the rising phase, 29 were randomly selected for model calibration. This process was repeated 10^4 times and the Mean Square Error (MSE) and equation coefficients (x and y) were recorded, at each iteration (Figure 2).

Final model selection (most representative model based on MSE modal value) follows Augusto-Silva et al. (2014) procedure: i) constructing a histogram of MSE; ii) computing of mean and standard deviations of model's coefficients in the most frequent error interval; iii) ranking of coefficients in the range of mean ± standard deviation according to their MSE, iv) selecting the model with the smallest MSE.

The chosen model was validated using the 13 remaining samples (not used in the calibration process) and the final accuracy was assessed following the metrics: coefficient of determination (r^2), MSE and normalized root mean square error in percentage (%NRMSE).

Once the relationship between $S_{275\text{-}29}$ and a_{CDOM} (440) was modelled, another algorithm was calibrated and validated for estimating a_{CDOM} (440) from simulated MSI Rrs. .Based on the recent literature concern on distinguishing CDOM and Non-Algal Particle (NAP) contribution to the Rrs in complex environments (Matsuoka et al., 2009; Matsuoka et al., 2012). This study proposes a new model for estimating a_{CDOM} (440) based on the ratio between near infrared bands for removing NAP contribution from its inorganic fraction. The rational for introducing this ratio is the null signal of CDOM and the dominance of NAP in near infrared range (Kirk, 2011). Previous studies also have shown that the inclusion of bands at wavelengths >600 nm increases the accuracy of the CDOM estimation model (Chen et al., 2017; Zhu et al., 2014). Thus, to determine a_{CDOM} (440), the exponential of the ratio between bands 6 (λcentral wavelength (λcw)=740 nm) and 5 (λcw=705 nm) are subtracted from the exponential of the ratio between bands 2 (λcw=490 nm) and 3 (λcw =560 nm) (Equation 7):

$$a_{cdom}(440) = x \cdot e^{(B2/B3)} - (y \cdot e^{(B6/B5)} + z) \,, \qquad (5)$$

where, x, y and z are the coefficients. B2, B3, B5 and B6 are the MSI sensor simulated bands 2, 3, 5 and 6.

Monte Carlo simulation was similarly performed to select the most representative model for estimating a_{CDOM} (440) as a function of Rrs. The validation process also followed the same procedure previously described for the slope.

3 Results

3.1 Seasonal and spatial variability of CDOM

The highest amplitude of a_{CDOM} (440) in the entire data set (e.g. across all sites) occurred in March (1.22 to 5.46 m^{-1}) and April (1.60 to 5.97 m^{-1}), with averages of 2.56 and 3.01 m^{-1}, respectively. In July and August, the amplitude was smaller (1.32 to 2.03 m^{-1} and 1.27 to 2.19 m^{-1}, respectively) and both averaged below 2 m^{-1}. No spatial variation was observed in a_{CDOM} (440) within lake.

The water level during the sampling campaign in the rising and receding phase was almost the same (mean=30.04 ± 1.38 m). However, at the rising phase, high variability (CV=52.45%) of a_{CDOM} (440) occurred, while in the receding a_{CDOM} (440) variability (CV=14.74%) was much smaller.

The Kruskal Wallis test using samples from all lakes and dates indicated that there are significant differences ($p<0.001$) in a_{CDOM} (440) between lakes and hydrograph phases. After the removal of Buabuá and Mamirauá samples acquired in March and April (rising), Kruskal Wallis results showed no significant differences in a_{CDOM} (440) values ($p=0.51$). The two runs indicate that DOM at Buabuá and Mamirauá, during the rising phase have a much higher absorption at 440 nm than those of the remaining lakes and months.

3.2 CDOM absorption spectra

The entire set of a_{CDOM} spectra (Figure 4) can be divided in two groups. The first group comprises Buabuá and Mamirauá spectra acquired at the rising phase, with a_{CDOM} at 254 nm ranging between 65 and 95 m^{-1}. The second group is composed by the Pantaleão and Pirarara spectra at rising phase and the samples of all the lakes acquired during the receding phase, with a_{CDOM} at 254 nm almost three times smaller, ranging from 26 to 35 m^{-1}. It is also noticeable the presence of shoulder between 245 and 290 nm in the absorption spectra (black arrow in Figure 4). Thus, during the rising phase there are differences between the spectra collected in the lakes surrounded by the flooded forest and those near the river. During the receding phase, however, this difference no longer exists, and all spectra have lower a_{CDOM} (254) values.

The analysis of average $S_{275\text{-}295}$ of each hydrograph phase also indicates the existence of differences between both, phases and lakes (Figure 5). The scatter plot displays the presence of two distinct groups: one including Mamirauá and Buabuá samples, and the other, Pantaleão and Pirarara. $S_{275\text{-}295}$ in all samples from Buabuá and Mamirauá are near or under 0.015 nm^{-1} in rising phase and equal or higher than 0.016 nm^{-1} in the receding phase. However, $S_{275\text{-}295}$ in all Pantaleão and Pirarara samples are above 0.015 nm^{-1} in the rising phase and below 0.0155 nm^{-1} in the receding phase, except for one single sample from Pantaleão. The significant relationship between $S_{275\text{-}295}$ and S_R indicates that these parameters can be tracking similar pools of DOM (Hansen et al., 2016). S_R same as $S_{275\text{-}295}$ indicates differences between the lakes surrounded by flooded forest and those near the river (see supplementary material S.1). Since $S_{275-295}$ also has been applied in remote sensing studies (Fichot et al., 2013; Vantrepotte et al., 2015), the present study has focused in modelling $S_{275-295}$.

3.3 Seasonal relationship between a_{CDOM} and $S_{275-295}$

The model proposed by Vantrepotte et al. (2015) was tested using the entire data set (coefficients of equation 0.05, 0.10, 3.06 and 0.0), but a power-law function provided a better fit (Figure 6).

The relationship between a_{CDOM} (440) and $S_{275-295}$ varies between hydrograph phases (Figure 7). As in the receding phase a_{CDOM} values are very similar among lakes and there is no apparent correlation between a_{CDOM} (440) and $S_{275-295}$, the model was developed only for the rising phase. The selected model to estimate $S_{275-295}$ from a_{CDOM} (440), developed using Monte Carlo and data from rising phase, shows a satisfactory fit (MSE<0.0001) and is described in Equation 6:

$$S_{275-295} = 0.016\, a_{CDOM}(440)^{-0.064}, \qquad (6)$$

Validation results showed a good explanation of the model´s variance (r^2=0.8) and predicted values close to observed values (%NRMSE=9.4), indicating the feasibility of estimating $S_{275-295}$ from a_{CDOM} (440) (Figure 8a). In the rising water, however, predicted $S_{275-295}$ diverges from the 1:1 line for values above ~0.015 nm^{-1}, indicating that the model is better parameterized for values of $S_{275-295}$ smaller than 0.015 nm^{-1}.

Once the relationship between a_{CDOM} (440) and $S_{275-295}$ was established for rising water, the model for estimating a_{CDOM} (440) based on Rrs was also calibrated for this period (Equation 7). The final model had provided MSE=0.65 m^{-1}:

$$a_{CDOM}(440) = 4.39^{\frac{B_2}{B_3}} + 0.59^{\frac{B_6}{B_5}} - 6.67, \qquad (7)$$

Model validation (Figure 8b) shows that almost 70% of the estimated values are within the 95% confidence interval and the statistics parameters (r^2, MSE and %NRMSE) present good accuracy in the estimation of a_{CDOM} (440).

4 Discussion

The variability of a_{CDOM} (440), a_{CDOM} spectra and $S_{275-295}$ along the hydrological year (Figures 1, 3, 4 and 5) indicated that these parameters are related to the hydrograph phases and lake geographical location in the floodplain. Mamirauá and Buabuá lakes are located in the middle of the floodplain, far from both main rivers, Solimões and Japurá and surrounded by High and Low Várzea Forests (Ferreira-Ferreira et al., 2015 Figure 5). While Pantaleão and Pirarara are lakes located near to Japurá River, subjected to both river inputs and Solimões River flood pulse.

The water level in the floodplain is quite similar between the rising and receding seasons, suggesting that the flood pulse is the major factor explaining the variability of those optical variables. The Solimões flood pulse phase is, therefore, the key variable controlling the variability of CDOM index. During the rising water level, the Solimões inflow into the floodplain as overland flow crosses a large area of forest and carries a considerable amount of organic matter in different stages of decomposition into Buabuá and Mamirauá lakes. Pantaleão and Pirarara lakes, however, are far from Solimões, being connected to Japurá

River located in the eastern extreme of the floodplain; therefore they are not affected by the Solimões overland flow in the beginning of the rising phase, receiving a minor input of organic matter as Buabuá and Mamirauá (Table 1).
As the study area consists entirely of a floodplain, that is subject to marked seasonal flooding (about 12 m), during the high water the entire ecosystem is flooded (Affonso et al., 2011). According to Ferreira-Ferreira et al. (2015), the entire area showed in Figure 1 is flooded for periods of up to 295 days in a year depending on the flood peak. In this study, the high-water phase was not sampled considering that previous studies (Affonso et al., 2011) indicated that during the high water all water bodies become interconnected with the main channels and rivers displaying the lowest spatial variability in all limnological variables, including DOC concentration. Actually, DOC coefficient of variation among sampled water bodies dropped from 53.87% in the low water to 20.89% in the high-water of 2009 hydrological year (Affonso et al., 2011). Considering that in the Amazon basin, DOC accounts for 70% of total organic matter and that floodplain areas are relevant sources of DOC to the Solimões/Amazon River (Morreira-Turq et al., 2003), in the present study we assume that it is possible that the differences in CDOM optical properties among Mamirauá/Buabuá and Pirarara/Pantaleão are related to the fact that the flood wave have not reached the eastern margin of the floodplain at the onset of the rising water phase.

In the rising phase, the water coming mainly from the Solimões river undergoes overbank flooding (Figure 1c), overtopping its channel and flowing across the litter through the forest before reaching the lakes (Junk, 1989). The tree-DOM accumulated during the lower water season may be an import source of organic matter to the lakes during this event (Van Stan and Stubbins, 2018). As explained in the previous paragraph, at beginning of the rising phase, the water from Solimões does not reach all the floodplain lakes at the same time. Therefore, in this period, DOM is expected to have significant differences between those lakes surrounded by flooded forests located near the Solimões River and those connected to Japurá River, located in the extreme eastern boundary of the study area. During the rising water phase, the water path to Pirarara and Pantaleão through the flooded forest is small, because they are closely connected to Japurá River. At that time, the Solimões overbank flood of the high-water season, responsible for homogenizing limnologic properties in floodplain lakes have not occurred yet (Abdo and Silva, 2004; Almeida and Melo, 2009; Carvalho et al., 2001; Henderson, 1999; Queiroz, 2007).

Regarding the assessment of $S_{275\text{-}295}$ values in this study (Figure 5), differences were found between both, lakes and hydrograph phases. During the rising phase, Pantaleão and Pirarara have higher $S_{275\text{-}295}$ (>0.015 nm^{-1}) than those of Buabuá and Mamirauá (<0.015 nm^{-1}), suggesting that DOM at lakes near that river have lower molecular weight (LMW) than those surrounded by forest. Also, high molecular weight (HMW) can be an indicative of allochthonous DOM since it is composed of refractory compounds such as lignin and cellulose. These results agree with previous studies indicating the presence of HMW DOM during rising water (Melo et al., 2019; Shen et al., 2012; Spencer et al., 2008). However, in the present study the authors do not have data to corroborate the optical analyses regarding the origin and molecular weight of DOM.

In our study, no significant correlation between a_{CDOM} (440) and $S_{275\text{-}295}$ was found for the data set including samples acquired in all hydrograph phases. During the receding water phase it is difficult to draw conclusions regarding DOM origin, since the DOM present in the lakes can be old and highly degraded (Wagner et al., 2019). During the rising phase, a significant correlation between a_{CDOM} (440) and $S_{275\text{-}295}$ can be found. This means that high (low) a_{CDOM} (440) values correspond to low (high) $S_{275-295}$ values, suggesting the presence of HMW (LMW) substances. In this way, it seems that a_{CDOM} (440) and $S_{275-295}$ are optical absorption indices that can be used to trace different CDOM dynamics between lakes and hydrograph phases in floodplain lakes. Since literature shows that these indices can be estimated via remote sensing data (Brezonik et al., 2015; Vantrepotte et al., 2015), their relationship with remote sensing reflectance (Rrs) was tested. However, because of the differences in CDOM dynamic among hydrography phases, only the relationship between the variables for the data set sampled during rising water could be modelled. Nonetheless, this hydrography phase is a key moment when the floodplain receives large amount of water coming from different Amazon drainage basin habitats which washes the floodplain floor and carries large amount of organic matter accumulated along the hydrological year.

There are several models relating a_{CDOM} (440) and remote sensing data in literature, but being empirical they are environmentally and seasonally dependent (Zhu et al. 2015). Kutser et al., (2016) tried to calibrate a model using data from Estonian lakes, Três Marias Reservoir (Brazil) and a floodplain lake located in Amazon (Curuai Lake). However, they were not able to fit a model describing the entire data set, what indicates that model development depends on DOM quality and degradation dynamics (Hansen et al., 2016). Models available in literature usually use the ratio between green and red bands (Toming et al., 2016; Zhu et al., 2014). In this study, we tested the correlation between a_{CDOM} (440) values and the ratio between the green and red bands, but the results were poor (see supplementary material S.2). Thus, we proposed a new model to estimate a_{CDOM} (440), using additional bands (Equation 7).

Despite the small number of samples, this study shows that it is possible to estimate $S_{275-295}$ from a_{CDOM} (440) during one crucial hydrography phase (rising phase), notwithstanding their hydrodynamic differences. Both the MSE and %NRMSE (<0.0001 m^{-1} and 9.40%) computed in this study are in the range of models available in the literature (Vantrepotte et al., 2015; Fichot et al., 2013), showing potential for estimating $S_{275-295}$ from a_{CDOM} (440). Therefore, a model for a_{CDOM} (440) estimation was also proposed. The a_{CDOM} (440) model also provided MSE and %NRMSE (0.53 m^{-1} and 15.12%) which is considered as an accurate estimate considering the various uncertainties related to remote sensing methods. Those modelling results, therefore, are encouraging suggesting that MSI images, when available, might be applied for studying DOM properties of the Amazon floodplain lakes during the rising water level. However, the models have limitations, which are: 1) its empirical nature demand calibration for application in other datasets; and 2) the small range of a_{CDOM} sampled (1.2 to 6.0 m^{-1}) and $S_{275-295}$ (0.0142 to 0.0165 nm^{-1}), indicating the need of new experiments including a larger number of lakes spread in a wider range of distance from the Solimões bank, a wider span of the rising hydrograph phase and DOM molecular analyses in order to validate the optical indices.

5 Conclusions

The present study indicates that the use of the optical indices, a_{CDOM} and $S_{275-295}$, provided a deeper understanding on the connections between Solimões and Japurá river flood pulse and DOM dynamics in the Amazon floodplain lakes. The results corroborates the findings in the most recent literature and indicates that there is an urgent need of research to explore new types of indices integrating both, optical spectral properties and remote sensing data.

The empirical model relating Rrs and a_{CDOM} (440); a_{CDOM} (440) and $S_{275-295}$ provided robust statistics indicating the high potential of MSI sensor for estimating $S_{275-295}$ during the rising water. Even though this study is the first attempt of using simulated MSI data to estimate $S_{275-295}$ in Amazon floodplain lakes, the results herein discussed seem very promising particularly considering the new generation of satellite-borne sensors with higher temporal resolution and the resources (costs and time) involving DOM analysis in laboratory.

Author contributions. MPdaS, LASdeC, EN and CCFB planned and designed the research. DSFJ and CCFB carried out parts of the field work and conducted a first version of data processing. MPdaS did the statistical analysis and wrote the paper with contributions from all co-authors.

Competing interests. The authors declare that they have no conflict of interest.

Acknowledgements. This study was funded by São Paulo Research Foundation (FAPESP 2014/23903-9), National Council for Scientific and Technological Development (CNPq 461469/2014-6 and CNPq 304568/2014-7) and by the project “Environmental Monitoring by Satellite in the Amazon Biome” from the Brazilian development bank (MSA-BNDES 1022114003005). Da Silva was funded by the CNPq (131242/2016-4). We are very grateful to Vitor Martins, Renato Ferreira, Jean Farhat, Franciele Sarmento, and Dr. Waterloo Pereira Filho for their assistance during field missions. We would like to thank Dr. Helder Queiroz and the Mamirauá Institute for all the support. We also would like to thank Dr. Otávio Cristiano Montanher for the correction of flow rate data and Dr. Ivan Bergier for suggestions. We would like to thank the reviewers for their thoughtful comments and efforts towards improving our manuscript.

References

Abdo, M. S. A., Silva, C. J. Limnological characteristics of the water bodies of the Corutuba Nesting Site in Brazil's Pantanal. Acta Limnologica Brasiliensia, 6 (4), 359-368, 2004.

Affonso, A. G., Queiroz, H. L. DE, Novo, E. M. L. D. M. Limnological characterization of floodplain lakes in Mamirauá Sustainable Development Reserve, Central Amazon (Amazonas State, Brazil). Acta Limnologica Brasiliensi, 23 (1), 95–108, 2011.

Almeida, F. F., Melo, S. Limnological considerations about an Amazonian floodplain lake (Catalao lake--Amazonas State, Brazil)/Consideracoes limnologicas sobre um lago da planicie de inundacao amazonica. Acta Scientiarum, 31 (4), 387-396, 2009.

Agencia Nacional de Aguas (ANA). Hidroweb < http://www.snirh.gov.br/hidroweb/>

Augusto-Silva, P. B., Ogashawara, I., Barbosa, C. C. F., DE Carvalho, L. A. S., Jorge, D. S. F., Fornari, C. I., Stech, J. L. Analysis of MERIS reflectance algorithms for estimating chlorophyll-a concentration in a Brazilian reservoir. Remote Sensing, 6 (12), 11689–11707, doi: https://doi.org/10.3390/rs61211689, 2014.

Ayres, J. M. As matas de várzea do Mamirauá. Conselho Nacional de Desenvolvimento Científico e Tecnológico. Sociedade Civil Mamirauá, Tefé, Brasil, 99 pp, 1995.

Brezonik, P. L., Olmanson, L. G., Finlay, J. C., Bauer, M. E. Factors affecting the measurement of CDOM by remote sensing of optically complex inland waters. Remote Sensing of Environment, 157, 199–215. https://doi.org/10.1016/j.rse.2014.04.033, 2015

Bricaud, A., Morel, A., Prieur, L. Absorption by dissolved organic matter in the sea (yellow substance) in the UV and visible domains. Limnology and Oceanography, 26, 43–53. https://doi.org/10.4319/lo.1981.26.1.0043, 1981.

Bukata, R. P. J., Jerome, J. H., Kondratyev, K. Y., Pozdnyakov, D. V. Optical properties and remote sensing of inland and coastal waters. Boca Taton, Florida: CRC Press LLC, 362 p, 1995

Carvalho, P., Bini, L. M., Thomaz, S. M., Oliveira, L. G., Robertson, B., Tavechio, W. L. G., Darwisch, A. J. Comparative limnology of South American floodplain lakes and lagoons. Acta Scientiarum Maringa, 23 (2), 256-273, 2011.

Castello, L., Viana, J. P., Watkins, G., Pinedo-Vasquez, M., Luzadis, V. A. Lessons from integrating fishers of arapaima in small-scale fisheries management at the Mamirauá Reserve, Amazon. Environmental Management, 43 (2), 197–209. https://doi.org/10.1007/s00267-008-9220-5, 2009.

Chen, J., Zhu, W. N., Tian, Y. Q., Yu, Q. Estimation of colored dissolved organic matter from landsat-8 imagery for complex inland water: case study of Lake Huron. Journal of Applied Remote Sensing, 11 (3), 1–12. https://doi.org/10.1109/tgrs.2016.2638828, 2017.

Coble, P. G. Marine optical biogeochemistry: the chemistry of ocean color. Chemical Reviews, 107 (2), 402–418. https://doi.org/10.1021/cr050350+, 2007

Cole, J. J., Prairie ,Y. T., Carcao, N. F., McDowell, W. H., Tranvik, L. J., Striegl, R. G., Duarte, C. M., Kortelainen, P., Downing, J. A., Middelburg, J. J, Melack, J. Plumbing the global carbon cycle: integrating inland waters into the terrestrial carbon budget. Ecosystems, 10 (1), 172-185. https://doi.org/10.1007/s10021-006-9013-8, 2007.

European Space Agency (ESA). User guides <https://earth.esa.int/web/sentinel/user-guides/sentinel-2-msi/resolutions/spatial> Access in: June 23, 2018.

Ferreira-Ferreira, J., Silva, T.S.F., Streher, A.S. Affonso, A.G., Furtado, L. F.A., Forsberg, B. R., Valsecchi, J., Queiroz, H. L., Novo, E. M. L. M. Combining ALOS/PALSAR derived vegetation structure and inundation patterns to characterize major vegetation types in the Mamirauá Sustainable Development Reserve, Central Amazon floodplain, Brazil. Wetlands Ecol Manage (2015) 23: 41. https://doi.org/10.1007/s11273-014-9359-1, 2015.

Fichot, C. G., Kaiser, K., Hooker, S. B., Amon, R. M., Babin, M., Bélanger, S., Walker, S. A., Benner, R. Pan-Arctic distributions of continental runoff in the Arctic Ocean. Scientific reports, 3, 1053. https://doi.org/10.1038/srep01053, 2013.

Hansen, A. M., Kraus, T. E. C., Pellerin, B. A., Fleck, J. A., Downing, B. D., Bergamaschi, B. A. Optical properties of Dissolved Organic Matter (DOM): effects of biological and photolytic degradation. Limnology and oceanography, 61 (3), 1015–1032. https://doi.org/10.1002/lno.10270, 2016.

Hastie, A, Lauerwald, R, Ciais, P, Regnier, P. Aquatic carbon fluxes dampen the overall variation of net ecosystem productivity in the Amazon basin: An analysis of the interannual variability in the boundless carbon cycle. Glob Change Biol. 25, 2094–2111, 2019.

Helms, J. R., Stubbins, A., Ritchie, J. D., Minor, E. C., Kieber, D. J., Mopper, K. Absorption spectral slopes and slope ratios as indicators of molecular weight, source, and photobleaching of chromophoric dissolved organic matter. Limonology and Oceanography, 53 (3), 955–969. https://doi.org/10.4319/lo.2008.53.3.0955, 2008.

Henderson, P.A. O ambiente aquático da Reserva Mamirauá. In: QUEIROZ, H. L. & CRAMPTON, W. G. R. (Eds.). Estratégias de Manejo de recursos Pesqueiros em Mamirauá. SCM, MCT-CNPq. Brasília, Cap. 1, p. 1-9, 1999.

Jaffé, R., McKnight, D., Maie, N., Cory, R., McDowell, W. H., Campbell, J. L. Spatial and temporal variations in DOM composition in ecosystems: The importance of long-term monitoring of optical properties. Journal of Geophysical Research: Biogeosciences, 113 (G4), 2008.

Jorge, D. S. F., Barbosa, C. C., Affonso, A. G., Novo, E. M. L. DE M. Spatial-temporal characterization of optical properties of 4 lakes in the Mamirauá Sustainable Development Reserve - AM (MSDR). In: Anais XVIII Simpósio Brasileiro de Sensoriamento Remoto, Santos - SP, 2017a.

Jorge, D. S. F., Barbosa, C. C., Carvalho, L. S. DE, Affonso, A. G., Lobo, F. DE L., Novo, E. M. L. de M. SNR (signal-to-noise ratio) impact on water constituent retrieval from simulated images of optically complex amazon lakes. Remote Sensing, 9 (7), 644. https://doi.org/10.3390/rs9070644, 2017b.

Junk, W. J., Bayley, P. B., Sparks, R. E. The flood pulse concept in river-floodplain systems. In: D.P. DODGE, ed. Proceedings of the International Large River Symposium. Ottawa: Canadian Government Publishing Centre, pp. 110-127. Special Publication of the Canadian Journal of Fisheries and Aquatic Sciences, no. 106, 1989.

Kirk, J. T. O. Light and photosynthesis in aquatic ecosystems. 3.ed. Cambridge, England: Cambridge University Press, 528 p, 2011.

Kutser, T.; Pierson, D. C.; Kallio, K. Y.; Reinart, A.; Sobek, S. Mapping lake CDOM by satellite remote sensing. Remote Sensing of Environment, v. 94, n. 4, p. 535-540, 2005.

Kutser, T., Casal Pascual, G., Barbosa, C., Paavel, B., Ferreira, R., Carvalho, L., Toming, K. Mapping inland water carbon content with Landsat 8 data. International Journal of Remote Sensing, 37 (13), 2950-2961, 2016

Li, P., Hur, J. Utilization of UV-Vis spectroscopy and related data analyses for dissolved organic matter (DOM) studies: A review. Critical Reviews in Environmental Science and Technology, 47 (3), 131-154, 2017.

Maia, C. M., Volpato, G. L. Environmental light color affects the stress response of Nile tilapia. Zoology, 116 (1), 64-66, https://doi.org/10.1016/j.zool.2012.08.001, 2013.

Mamirauá Institute of Sustainable Development. Database of fluviometric data from Mamirauá Sustainable Development Reserve< http://mamiraua.org.br/pt-br/pesquisa-e-monitoramento/monitoramento/fluviometrico/> Access in: June, 23, 2018.

Matsuoka, A.; Larouche, P.; Poulin, M.; Vinvent, W.; Hattori, H. Phytoplankton community adaptation to changing light levels in the southern Beaufort Sea, Canadian Arctic, Estuarine, Coastal and Shelf Science, 82, 537-546, 2009.

Matsuoka, A.; Bricaud, A., Bennerm R.; Para, J.; Sempéré, R.; Prieur, L.; Bélanger, S.; Babin, M. Tracing the transport of colored dissolved organic matter in water masses of the Southern Beaufort Sea: relationship with hydrographic characteristics, Biogeosciences, 9, 925–940, 2012.

Melo, M. L., Kothawala, D. N., Bertilsson, S., Amaral, J. H., Forsberg, B., Sarmento, H. Linking dissolved organic matter composition and bacterioplankton communities in an Amazon floodplain system. Limnology and Oceanography, 9999, 1–14. doi:10.1002/lno.11250, 2019.

Mobley, C. D. Estimation of the remote-sensing reflectance from above-surface measurements. Appl. Opt., 38, 7442–7455, https://doi.org/10.1364/ao.38.007442, 1999.

Moreira - Turcq, P., Seyler, P., Guyot, JL e Etcheber, H. Exportation of organic carbon from the Amazon River and its main tributaries. Hydrol. Process. 17, 1329-1344, 2003

Mori, G.B., Schietti, J., Poorter, L., Piedade, M.T.F. Trait divergence and habitat specialization in tropical floodplain forests trees. PLoS ONE, 14 (2). https://doi.org/10.1371/journal.pone.0212232, 2019.

Mueller, J.L.; Fargion, G.S. Ocean Optics Protocols for Satellite Ocean Color Sensor Validation; Revision 3; NASA TM 2002-210004; NASA Goddard Space Flight Center: Greenbelt, MD, USA, 2002; p. 308.

Pangala, S. R., Enrich-Prast, A., Basso, L. S., Peixoto, R. B., Bastviken, D., Hornibrook, E. R. C., Gatti, L. V., Marotta, H., Calazans, L. S. B., Sakuragui, C. M., Bastos, W. R., Gloor, O. M. E., Miller, J. B., Gauci, V. Large emissions from floodplain trees close the Amazon methane budget. Nature, 552 (7684), 230–234. https://doi.org/10.1038/nature24639, 2017.

Queiroz, H. L. Classification of water bodies based on biotic and abiotic parameters at the várzeas of Mamirauá Reserve, Central Amazon. Uakari, 3, p. 19-34, 2007.

Richey, J. E., Melack, J. M., Aufdenkampe, A. K., Ballester, V. M., Hess, L. L. Outgassing from Amazonian rivers and wetlands as a large tropical source of atmospheric CO2. Nature, 416 (6881), 617-620. https://doi.org/10.1038/416617a, 2002.

Seekell, D. A., Lapierre, J.-F., & Cheruvelil, K. S. A geography of lake carbon cycling. Limnology and Oceanography Letters, 3(3), 49–56, 2018.

Shen, Y., Fichot, C. G., Benner, R. Floodplain influence on dissolved organic matter composition and export from the Mississippi-Atchafalaya River system to the Gulf of Mexico. Limnology and Oceanography, 57 (4), 1149-1160, 2012.

Spencer, R. G., Aiken, G. R., Wickland, K. P., Striegl, R. G., Hernes, P. J. Seasonal and spatial variability in dissolved organic matter quantity and composition from the Yukon River basin, Alaska. Global Biogeochemical Cycles, 22 (4), 2008.

Toming, K., Kutser, T., Laas, A., Sepp, M., Paavel, B., Noges, T. First experiences in mapping lake water quality parameters with Sentinel-2 MSI imagery. Remote Sensing, 8 (8), 1–14. https://doi.org/10.3390/rs8080640, 2016.

Tranvik, Lars J., Downing, John A., Cotner, James B., Loiselle, Steven A., Striegl, Robert G., Ballatore, Thomas J., Dillon, Peter, Finlay, Kerri, Fortino, Kenneth, Knoll, Lesley B., Kortelainen, Pirkko L., Kutser, Tiit, Larsen, Soren., Laurion, Isabelle, Leech, Dina M., McCallister, S. Leigh, McKnight, Diane M., Melack, John M., Overholt, Erin, Porter, Jason A., Prairie, Yves, Renwick, William H., Roland, Fabio, Sherman, Bradford S., Schindler, David W., Sobek, Sebastian, Tremblay, Alain, Vanni, Michael J., Verschoor, Antonie M., von Wachenfeldt, Eddie, Weyhenmeyer, G. A. Lakes and reservoirs as regulators of carbon cycling and climate, Limnology and Oceanography, 54, https://doi.org/10.4319/lo.2009.54.6_part_2.2298, 2009.

TRIOS. Trios sensor. 2018. Disponível em: https://www.trios.de/en/.

Vantrepotte, V., Danhiez, F. P., Loisel, H., Ouillon, S., Mériaux, X., Cauvin, A., Dessailly, D. CDOM-DOC relationship in contrasted coastal waters: implication for doc retrieval from ocean color remote sensing observation. Optics Express, 23 (1), 33. https://doi.org/10.1364/oe.23.000033, 2015.

Volpato, G. L., Duarte, C. R. A., Luchiari, A. C. Environmental color affects Nile tilapia reproduction. Brazilian Journal of Medical and Biological Research, 37, 479-483. https://doi.org/10.1590/s0100-879x2004000400004, 2004.

Wagner, S., Fair, J. H., Matt, S., Hosen, J. D., Raymond, P., Saiers, J., Shanley, J. B., Dittmar, T., Stubbins, A. Molecular Hysteresis: Hydrologically Driven Changes in Riverine Dissolved Organic Matter Chemistry During a Storm Event. Journal of Geophysical Research: Biogeosciences, 124 (4), 759-774, 2019.

Werdell, J., McKinna, L. I. W., Boss, E., Ackleson, S. G., Craig, S. E., Gregg, W. W., Lee, Z., Maritorena, S., Roesler, C. S., Rousseaux, C. S., Stramski, D., Sullivan, J. M., Twardowski, M. S., Tzortziou, M., Zhang, X. An overview of approaches and challenges for retrieving marine inherent optical properties from ocean color remote sensing. Progress in Oceanography, 160, 186–212. https://doi.org/10.1016/j.pocean.2018.01.001, 2018.

Zhu, W., Yu, Q., Tian, Y. Q., Becker, B. L., Zheng, T., Carrick, H. J. An assessment of remote sensing algorithms for colored dissolved organic matter in complex freshwater environments. Remote Sensing of Environment, 140, 766–778. https://doi.org/10.1016/j.rse.2013.10.015, 2014.

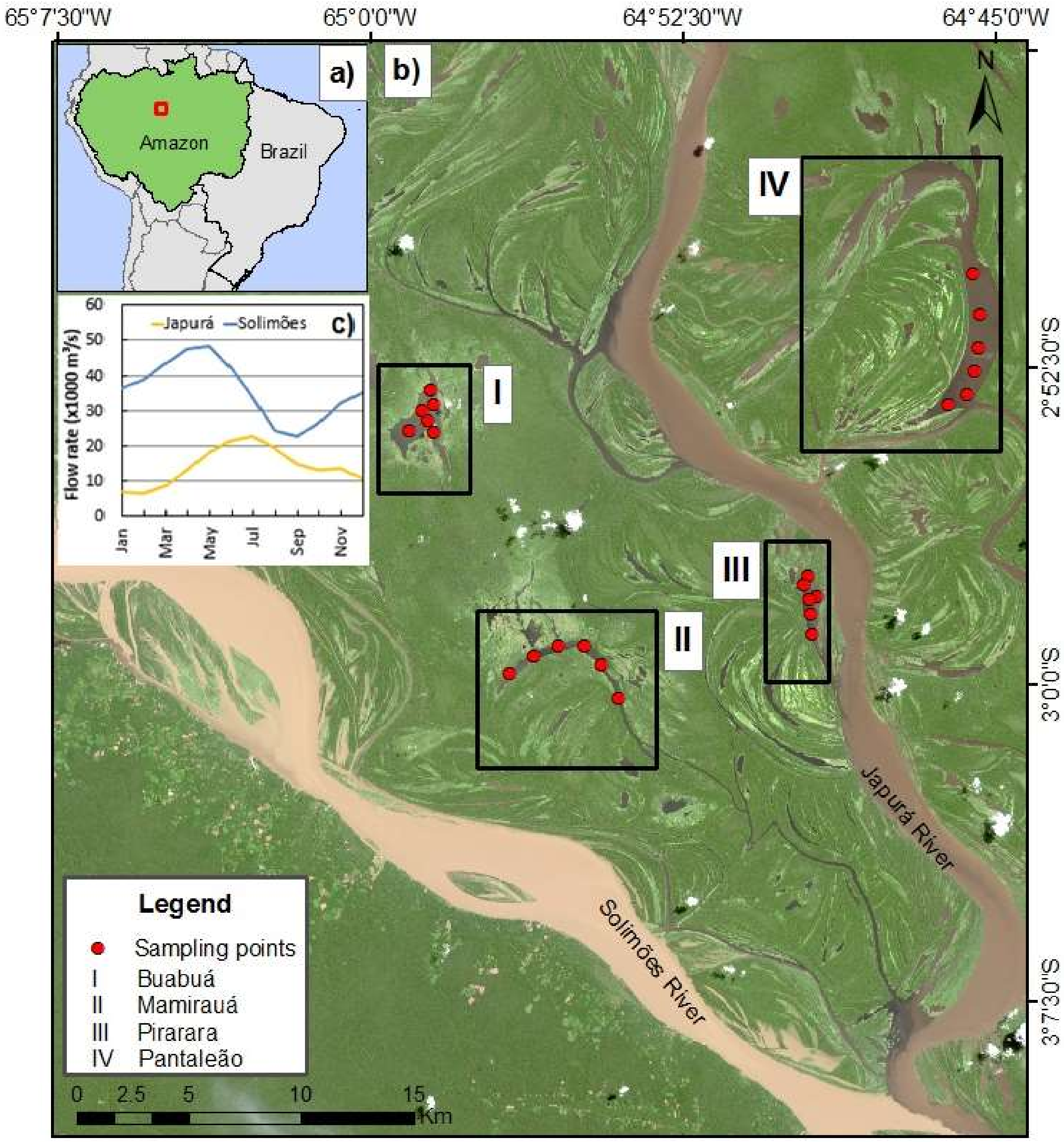

Figure 1 – Study area. (a) Overview Amazon. (b) OLI/ Landsat 8 true color image from July 30th of 2015 showing the study area and sample stations lakes: (I) Buabuá; (II) Mamirauá; (III) Pantaleão; and (IV) Pirarara. (c) Water flow rate at Japurá and Solimões rivers (Brazilian Water National Agency - ANA).

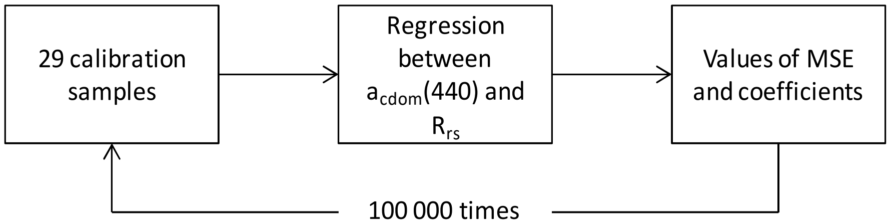

Figure 2 – Diagram of Monte Carlo simulation.

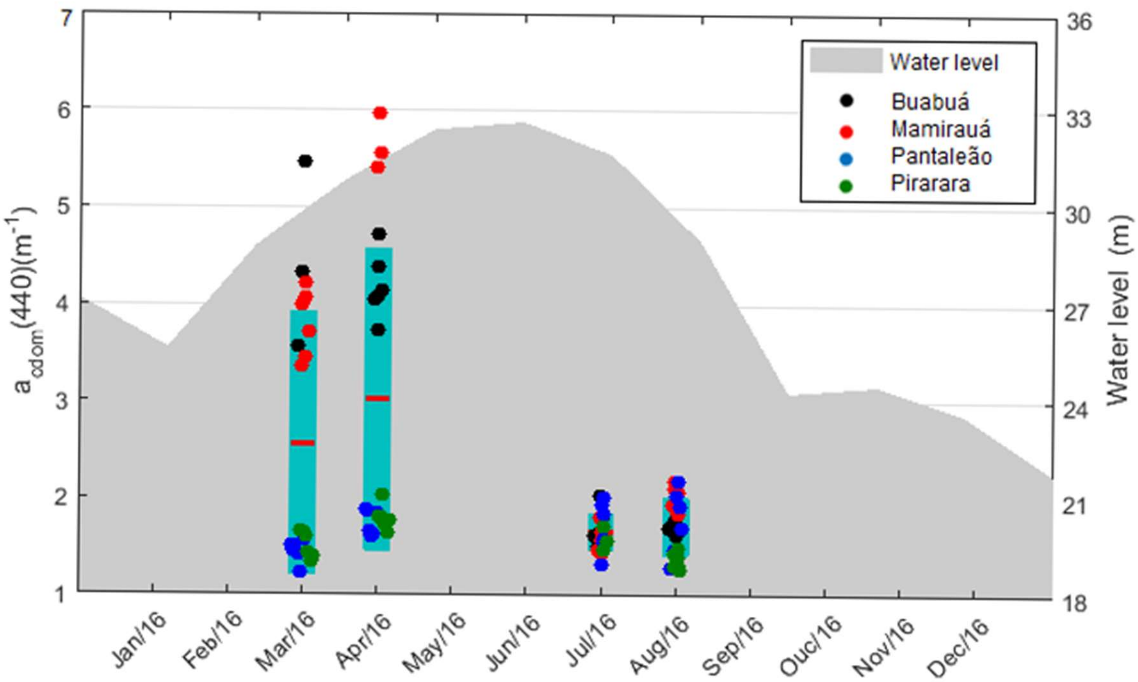

Figure 3 – Seasonal box-plot of a_{CDOM} (440) (m^{-1}) and water level (m) of Mamirauá channel in 2016. The red lines are the mean a_{CDOM} (440); each dot represent the a_{CDOM} (440) value at each sample station of lakes; and the blue boxes represent the interval between the first and third quartile. Water level data were acquired from Mamirauá Sustainable Development Institute (MISD, 2017).

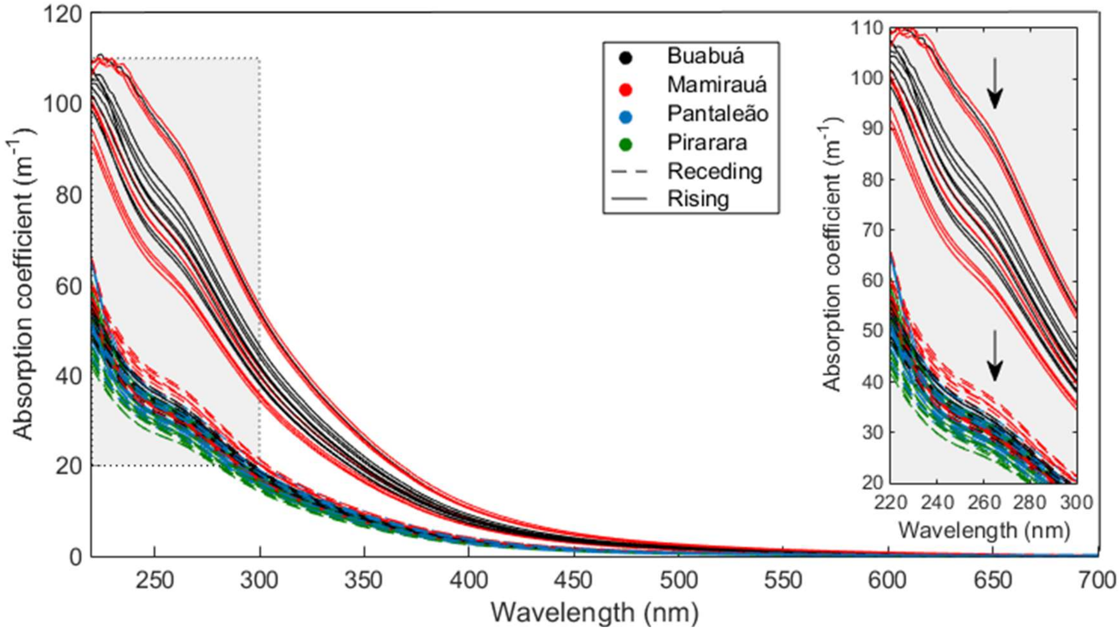

Figure 4 - a_{CDOM} absorption spectra collected in Buabuá (black), Mamirauá (red), Pantaleão (blue) and Pirarara (green) lakes during rising (solid line) and receding (dash line) water phase. The black arrows indicate the shoulder between 245 and 290 nm.

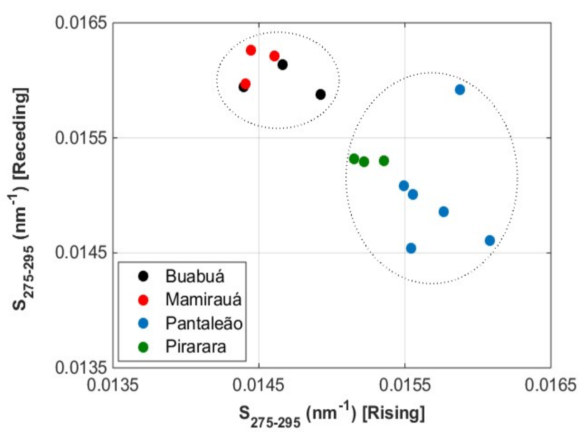

Figure 5 – Dispersion diagram of average $S_{275-295}$ (nm^{-1}) at each hydrograph phase (rising and receding) and in all lakes. The dotted ellipsis represents the two groups identified.

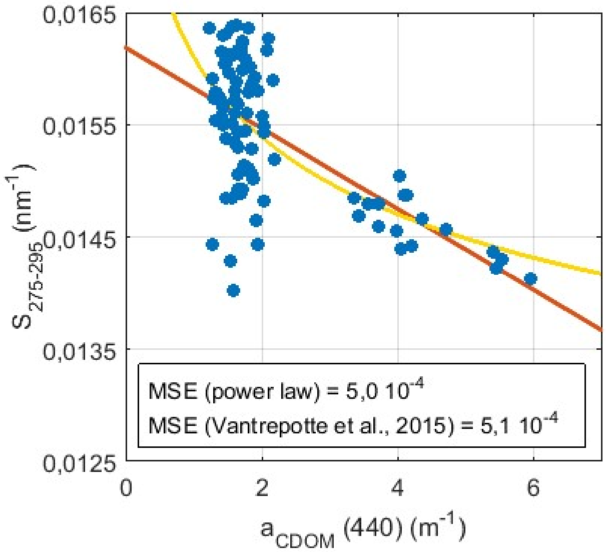

Figure 6 - Adjustment of the model proposed by Vantrepotte et al. (2015, Equation 7) (in red) and adjustment of the proposed power law model described in Equation 6 (in yellow).

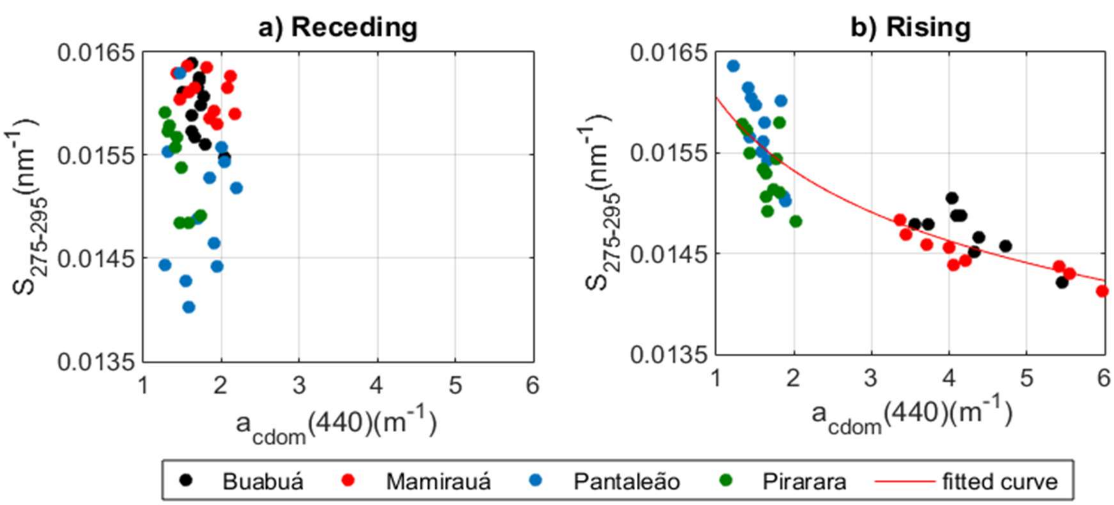

Figure 7 - Scatterplot of a_{CDOM} (440) (m^{-1}) versus $S_{275-295}$ (nm^{-1}) for a) receding and b) rising phases of the hydrograph.

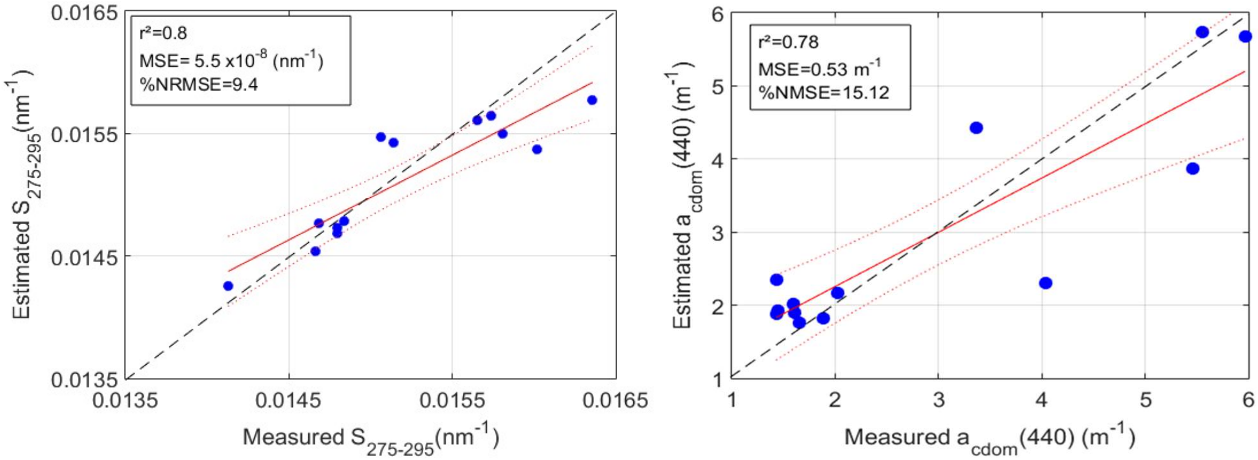

Figure 8 – Measured versus estimated scatterplot of (left) $S_{275-295}$ (nm^{-1}) and (right) a_{CDOM} (440) (m^{-1}). Equation 4 was used to estimate $S_{275-295}$ (Y axis). Equation 5 was used to estimate a_{CDOM} (440) (Y axis). The red solid line indicates the regression line between measured and estimated values; the red double dotted lines are the 95% confidence interval; and the black dashed line is the 1:1 line.

Table 1 – Overview of the sampling points.

Sampling point	DOC [mgL^{-1}]			
	Rising water		Receding water	
	March	April	July	August
Buabuá_1	9.0	7.2	4.0	4.7
Buabuá_2	10.1	8.3	3.9	4.0
Buabuá_3	7.6	7.7	4.0	4.2
Buabuá_4		8.2	3.8	4.1
Buabuá_5		7.7	4.1	4.0
Buabuá_6		8.1	3.9	3.9
Mamirauá_1	9.6	9.4	4.5	4.2
Mamirauá_2	7.4	9.5	4.5	3.7
Mamirauá_3	7.3	9.7	4.9	3.7
Mamirauá_4	8.0		4.3	4.2
Mamirauá_5	8.7		4.3	4.0
Mamirauá_6	7.7		4.5	4.0
Pantaleão_1	4.0	3.7	3.9	3.5
Pantaleão_2	3.8	4.4	3.8	3.3
Pantaleão_3	4.2	3.5	3.7	3.7
Pantaleão_4	4.0	3.6	4.1	4.0
Pantaleão_5	4.5	3.4	3.1	3.9
Pantaleão_6	4.8	3.5	3.1	4.0
Pirarara_1	3.8	3.7	3.9	4.7
Pirarara_2	8.7	3.4	3.5	3.9
Pirarara_3	3.7	3.4	3.9	4.0
Pirarara_4	3.7	3.7		3.9
Pirarara_5	3.7	3.4		3.9
Pirarara_6	5.2	3.5		4.8